Study of the differential cross section for the reaction $K_L p \to K_S p$ between 5 and 10 GeV/c incident momentum

Marshall Mugge,* David McQuate,† Robert Morse,‡ and Uriel Nauenberg
University of Colorado, Boulder, Colorado 80302

David Hitlin,§ Jasper Kirkby, and John Liu‖
Stanford Linear Accelerator Center, Stanford, California 94305

Paul Cowell,¶ Paul Condon, and Jonathan Dorfan**
University of California at Irvine, Irvine, California 92717

(Received 7 May 1979)

We discuss a measurement of the differential cross section for the reaction $K_L p \to K_S p$ for incident momenta between 5 and 10 GeV/c and the $|t|$ region 0.025 to 0.5 (GeV/c)^2, carried out using the SLAC 15-in. rapid-cycling hydrogen bubble chamber triggered by the K^0 spectrometer facility. This hybrid detector allowed measurement of the K_L beam momentum, measurement of the recoil-proton momentum, and measurement of the decay position and momentum of the K_S. Over this momentum region the ratio of the real to imaginary part of the forward-scattering amplitude was determined to be 0.93 ± 0.24 and the phase of the forward-scattering amplitude was determined to be $-(138 \pm 7)°$. A fit to the forward differential cross section of the form $d\sigma/dt \propto p^{2\alpha(t)-2}$ to our data together with previous measurements of the $K_L p \to K_S p$ differential cross section at this and lower momenta yielded an $\alpha(0) = 0.39 \pm 0.10$ for the dominant ω Regge trajectory. The value of $\alpha(0)$ as determined from the phase $\phi = -\pi[\alpha(0)+1]/2$ is 0.54 ± 0.11.

I. INTRODUCTION

One approach to the understanding of high-energy scattering experiments at low transverse momenta has been to view the interactions in terms of the exchange of a small number of particles. Regge extended the idea of the exchange of a particle to the exchange of a trajectory. This physically simple view of interactions where only one or two trajectories are exchanged has been remarkably successful. Recent measurements at Fermilab and CERN of the reactions $\pi^- p \to \pi^0 n$ and $\pi^- p \to \eta n$ were found to be well described by the Regge formalism for these processes in terms of the exchange of trajectories.[1]

It was pointed out by Gilman[2] that the process $K_L p \to K_S p$ offered the opportunity to study the exchange of only $J^p = 1^-$ states. The only particles fitting this description are the ω, ρ, and ϕ. Since the ϕ-N coupling is small,[3] we can expect that the ϕ- exchange contribution to this process can be neglected. In addition, since spin-flip amplitudes cannot contribute in the forward direction (specifically at $t=0$) we expect the ρ contribution for low t to be small. Hence a measurement of the differential cross section of the reaction $K_L p \to K_S p$ can be used to determine the ω-trajectory parameter $\alpha(t)$ in the small-transverse-momentum region.

The measurement described here was made using the 15-in. rapid-cycling bubble chamber (RCBC) placed in front of the K^0 spectrometer at SLAC.[4] The RCBC[5] was pulsed at 20 times per second with a central field of 10.4 kG. The spectrometer selected only those events which met the geometrical requirements defined by the reaction $K_L p \to K_S p$, namely two forward-going charged particles. When a likely candidate was detected, a picture was taken and all the spectrometer information was recorded on tape. Off-line analysis of the spectrometer information made further cuts that reduced the number of pictures that had to be viewed by the scanners. Only one third of the pictures taken had to be scanned. Two very useful features of this detector allowed us to remove the background and improve the resolution of the measurement. First, by using time of flight (TOF) we were able to determine the incident K_L momentum, and second, the forward spectrometer gave us a 1% momentum measurement of the secondary tracks from the K_S decay.

The final fitted data consist of 112 events in the momentum region 5–10 GeV/c and $|t|$ region 0.025–0.5 (GeV/c).[2] A Monte Carlo program was used to determine the trigger efficiency of the detector. The beam flux and shape were determined using $K_{\mu 3}$ decays. Details of the various aspects of the experiment are presented.

II. THE K^0 BEAM

The K^0's in the experiment were produced by the SLAC 20.5-GeV/c electron beam incident on a

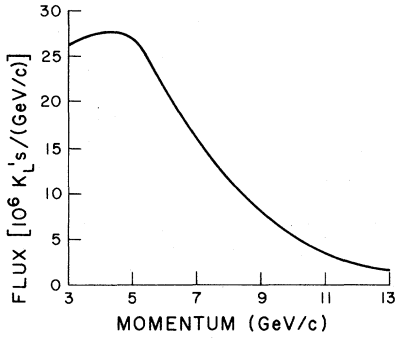

FIG. 1. The total flux of K_L at the bubble chamber as a function of momenta.

56-cm-long beryllium target. After passing through the target, the electrons passed through an induction loop, giving a well-defined time reference for both triggering and TOF purposes. The electron beam came in 1.6-μsec-long pulses. Each pulse consisted of 15-psec-wide bunches with a 25-nsec separation between them. The target was viewed at 3° relative to the incident electron direction. Charged and neutral secondaries passed through 25 cm of lead to remove photons and then through 61 cm of polyethylene to improve the K_L-to-neutron ratio. Sweeping magnets removed charged particles from the secondary beam.

The K_L momentum spectrum at the bubble chamber was determined by a detailed study of $K_{\mu 3}$ decays, making use of the timing information to resolve the two-fold kinematic ambiguity in the incident momentum determination. This determination is discussed in detail in Sec. V. The integral beam spectrum at the bubble chamber, which was 74 m from the target, is shown in Fig. 1.

III. EXPERIMENTAL DETAILS

The experimental setup is shown in Fig. 2.[4,6,7] Multiwire proportional chambers (MWPC) were placed in the walls of the bubble chamber and had both a fast and a delayed output which could be latched if a fast trigger requirement was met. The fast OR of the upstream MWPC (V) acted as a veto against charged tracks coming from the outside or being produced in the walls of the RCBC giving an acceptable trigger in the forward direction. The downstream MWPC (within the RCBC walls) was divided into a central region (Q) and two side regions (V_2, V_3) for use in the fast trigger logic. A Q signal was an indication that an interaction had taken place in the bubble chamber and a possible candidate of interest was emerging from the bubble chamber. A V_2 or V_3 signal indicated that the event was either a large-momentum-transfer event (unlikely) or, more likely, a multiprong event. Hence we used V_2 and V_3 as veto counters.

The reaction $K_L p \to K_S p \to \pi^+\pi^- p$ yielded two fast forward pions. These, after giving a signal in the Q counters, went through the T bank, which consists of 26 2-cm-wide scintillation counters. These counters were used to provide a 15-nsec time resolution in the trigger logic as compared to ~50 nsec for the Q counter. At the edges of the T bank, large scintillation counters V_4 and V_5 were placed as veto counters, reducing triggers due to large-transverse-momentum and multiprong interactions in the same manner as V_2 and V_3. At

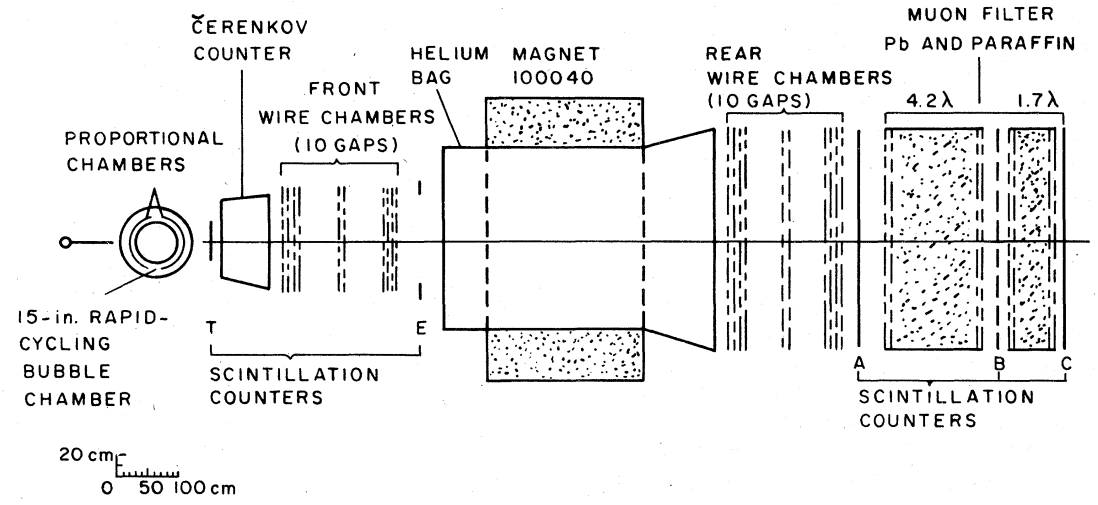

FIG. 2. A schematic view of the neutral-kaon spectrometer and the rapid-cycling bubble chamber.

least one T counter was required in the trigger. After these counters the forward tracks went through the upstream half of the spark-chamber system in the spectrometer. It consisted of four planes in the X and four planes in the Y views. There was also a diagonal pair to resolve the ambiguities. To make sure that the tracks went through the magnet, scintillation counters were placed along the aperture of the magnet (E). These were used in anticoincidence to remove likely multiprong events, or events with tracks which would not go through the magnet.

After the magnet the tracks went through the downstream half of the spark chambers which had the same number of planes as the upstream group. Finally, the tracks gave signals in the 16 scintillation counters that made up the A bank. At least two A counters were required in the trigger. The fast trigger was required to be in coincidence with a beam pulse (C). The logic that satisfied our trigger was $(C) \cdot (Q) \cdot (\geq 1T) \cdot (\geq 2A) \cdot (\overline{EV}_{12345})$.

If the fast trigger was satisfied, counters and MWPC were latched and spark chambers were pulsed. The MWPC latches were counted and if two or more groups of wires were latched, a second tier trigger was satisfied. Only then was a bubble-chamber picture taken. The counting and decision making took some 200 μsec and came well ahead of the 1.6 msec required for bubble expansion before a picture could be taken.

Periodic monitoring of various elements of the detector was carried out. The timing electronics was checked with light-emitting-diode pulser runs to calibrate the time-to-digital converters (TDC's). In addition, the electronic drifts and resolution were determined using muons from the target. The TDC scale, typically 0.135 nsec/bin, was determined with a light pulser. The muon runs allowed pulse-height corrections to the timing to be calculated both for the cable pulse height (from the target) that started the timing circuit and the A-counter pulse that stopped it. Study of four-constraint fits showed that the timing-resolution function was Gaussian with a standard deviation of 0.30 nsec.

IV. DATA REDUCTION

In the event that a picture was taken, all the spectrometer information was recorded on tape. The spectrometer chamber information was reconstructed in a straightforward manner. All three- and four-hit lines in the X view were matched with all three-and four-hit lines in the Y view. If any combination had a projected U-V hit which corresponded to a spark in the U-V planes, a track was declared as found. A χ^2 requirement for a quality of fit to a line and a restriction that no hit could be used more than twice were the only requirements placed on the lines. Tracks in the front and rear of the spectrometer were matched by distance of closest approach inside the momentum analyzing magnet.

All successful tracks were then ray traced back into the bubble-chamber visible region through its magnetic field using a fourth-order Runge-Kutta method. If the tracks came within 5 cm of each other, they were considered as intersecting and hence forming a vertex in the bubble chamber. Then the spectrometer information of these tracks, such as their momenta, counter times, probable vertex position, etc., were written on tape to be combined later with the measurements obtained from the bubble-chamber picture.

Scanning lists were generated with very loose scanning requirements. The scanners were given the X and Z locations and opening angle of the vertex as calculated by the spectrometer program. If a vertex was found in a band within ± 3 cm of the beam direction associated with the supposed vertex, that event was measured. These measurements were done with film-plane digitizers and they were put on magnetic tape.

The standard bubble-chamber program TVGP was used to process all the measured film data. The TVGP results were then compared with the spectrometer information and, if agreement was found, merged together. The definition of "agreement" reads as follows: A comparison of the projected vertices from the spectrometer data with that from the bubble-chamber data showed that the good events had a Gaussian distribution in both X and Y with a standard deviation of 0.27 cm. Hence the scanning requirement and final cut of ± 3 cm were more than adequate to pick out all the events. In Z (along the beam) the resolution was much poorer due to the multiple scattering of the tracks as they went through the walls of the bubble chamber and the small opening angle of the tracks at the vertex. Here we obtained a Gaussian distribution in Z with a standard deviation of 6.9 cm. No cuts in Z were applied at this stage.

After the data were merged, we had to match the bubble-chamber and spectrometer tracks. If the tracks in the bubble chamber were ~5 cm or longer, the charge of the track was clear in most instances and the matching was easily done. If this was not the case, then we carried out a comparison of the direction of the tracks. By comparing the angles, 97% of the events had an unambiguous match. The remaining 3% were resolved by letting the best of the possible matches be the right one. Once this was carried out, the spectrometer values for the momentum and the associated error of each track replaced the TVGP value.

The angular determination of the tracks at the vertex using the spectrometer information was added in quadrature with the TVGP measurements and the result placed in the TVGP record. Finally, a beam track was placed in the TVGP record with the directions determined by the target and interaction vertex positions and the momentum determined by the TOF.

The data were then sent through the kinematic-fitting program SQUAW to test for energy and momentum conservation. The events which were considered to contain a K_S decay and a recoil track were sent through the program with the following hypotheses as trials: (1) $K_L p \to K_S p$, (2) $K_L p \to K_S \pi^0 p$, (3) $K_L p \to K_S \pi^+ n$, (4) $\bar{K}^0 p \to \Lambda \pi^+$.

V. THE BEAM FLUX AND MOMENTUM SPECTRUM

To measure the cross section we had to determine the flux of the incident K_L's. A unique aspect of this experiment was that the data necessary to determine the beam shape and the flux were recorded simultaneously with the normal data because the decay $K_L \to \pi\mu\nu$ satisfied the trigger. Hence no special runs with a modified trigger or equipment were needed. The $K_L \to \pi\mu\nu$ decay produced two fast forward tracks which passed through the spectrometer. The muons with enough energy passed through the lead wall at the end of the spectrometer (See Fig. 2), giving a B and C latch. A Monte Carlo[8] simulation was used to determine the geometrical efficiency of the detector for $K_{\mu 3}$ decays. To get the actual beam momentum spectrum, an expected beam spectrum was put in the program, the decays were generated, sent through the spectrometer, and, for those which triggered the detector, the momentum was reconstructed. There were, typically, two possible momentum values. By converting these solutions to a TOF, they could be compared to the measured TOF and the worst solution rejected. The generated momentum spectrum was then compared to the measured one. The input expected beam spectrum was modified until the Monte Carlo and measured beam spectrum agreed. The final comparison is shown in Fig. 3 and the correct input spectrum is shown in Fig. 1.

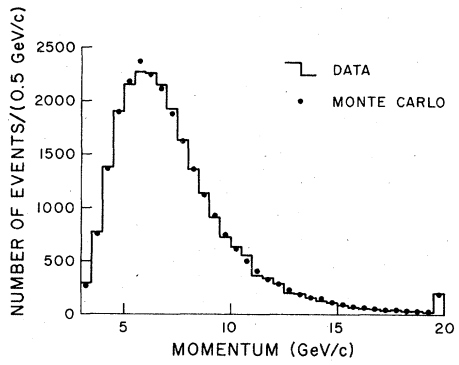

FIG. 3. Sample distribution showing the agreement between the data and the Monte Carlo simulation. Many other measured distributions were checked with the Monte Carlo simulation and agreement in all cases was very good.

A number of requirements were made before an event was declared to be a $K_{\mu 3}$. The event had to be composed of a positive and negative track, and one track had to satisfy the hadron trigger, while the other had to satisfy the muon trigger. A track was considered a muon if the momentum was greater than 1.8 GeV/c and had a B-counter latch within one counter of its projected position and a C-counter latch within two counters of its pro-

TABLE I. Summary of $K_{\mu 3}$ requirements.

1. The vertex must be within ±35 cm of the center of the bubble chamber.
2. The vertex must be composed of one positive and one negative track.
3. One track must be a muon, the other track must not be a muon.
4. Maximum combined mass of the tracks, treating both as pions, was 0.541 GeV/c^2.
5. Maximum transverse momentum to the beam of the individual tracks was 0.238 GeV/c.
6. Maximum transverse momentum to the beam of the two charged tracks combined was 0.207 GeV/c.
7. Allowed range of $P_0'^2$ was -9.99 to 0.050 GeV^2/c^2. P_0' is the momentum of the kaon in the frame where the sum of the longitudinal components of the charged decay products treated as pions is zero.
8. Times of the two tracks at the bubble chamber had to be within 1.5 nsec of each other.

jected position. A hadron was a track with a momentum less than 1.2 GeV/c or a momentum greater than 1.2 GeV/c and no B-counter and C-counter latch. Given that a pair of tracks satisfied these criteria, a number of additional kinematical and geometrical cuts was made before a decay was accepted. This was done to remove the background from other K_L decays. These requirements or cuts are summarized in Table I.

The background in this $K_{\mu 3}$ sample due to other decays was determined with the Monte Carlo spectrum. $K_{\pi 3}$, K_{e3}, and $K_{\pi 2}$ events were generated. The resulting pions in these final states could decay while traversing the spectrometer giving a reconstructed event which could satisfy the $K_{\mu 3}$ cuts shown in Table I. Using a Monte Carlo sample where the beam was allowed to decay into the various modes with the known branching ratios, we determined that of all the reconstructed "$K_{\mu 3}$ events", 92.8% were actually $K_{\mu 3}$, 3.8% were $K_{\pi 3}$, 3.3% were K_{e3}, and 0.1% were $K_{\pi 2}$. This background was corrected for in the determination of the beam spectrum.

To obtain the K_L beam flux we carried out a scan for V's on 15% of the approximately 800 000 pictures which were obtained in the experiment. This yielded 1604 $K_{\mu 3}$ decays in a ±16-cm fiducial region out of a total 3724 $K_{\mu 3}$'s that triggered the spectrometer and were on the tapes. The difference was due to decays that occurred in the nonvisible portion of the hydrogen volume. Using this ratio we determined an effective number of visible $K_{\mu 3}$ decays in the entire experiment to be 10 345. After taking into account the geometric detection efficiency, background from other decay modes, and possible systematic errors, we determined that the total number of K_L decays in the ±16-cm fiducial region of the bubble chamber was $(2.682 \pm 0.066) \times 10^5$. Using the now known beam spectrum and the K_L decay probability we obtained the K_L flux shown in Fig. 1.

VI. DATA ANALYSIS AND RESULTS

To determine the final differential cross section, several corrections were necessary. The Monte Carlo simulation included details of the bubble-chamber geometry, its magnetic field, and the effects of multiple scattering and interactions in the walls. The effect of pion decay, multiple scattering, and spark jitter was part of the track propagation through the spectrometer. Events so generated were analyzed with the same program as were the real data. The same cuts and requirements were applied to both sets of data in order to determine the geometrical efficiency. Shown in Table II is the efficiency as a function of incident momentum and momentum transfer. Systematic corrections were made for losses due to a Z cut used in some of the data (1.21 ± 0.03) and losses due to kinematical reconstruction requirements (1.02). Also, corrections were made for differences between $K_{\mu 3}$ and $K_L p \to K_S p$ events in their track failure rates (1.06 ± 0.01) and scanning efficiencies (1.02 ± 0.06). An additional correction was made for loss of the unobserved decay $K_S \to \pi^0\pi^0$ (1.456 ± 0.005).

It was necessary to isolate a clean and meaningful sample of $K_L p \to K_S p$. Only fits with a kinematical χ^2 probability greater than 2% were con-

TABLE II. Differential cross section $d\sigma(p,t)/dt$ for $K_L p \to K_S p$.

$-t$ (GeV$^2/c^2$)	$\frac{d\sigma}{dt}\left(\frac{\mu b}{(GeV^2/c^2)}\right)$	Number of events	Monte Carlo efficiency
	Momentum region 5.0–7.5 GeV/c		
0.025–0.050	198 ±50	17	0.1119
0.050–0.100	141 ±33	21	0.0968
0.100–0.150	114 ±33	13	0.0742
0.150–0.250	67 ±21	11	0.0535
0.250–0.350	57 ±24	6	0.0345
0.350–0.500	33 ±19	3	0.0196
		71	
	Momentum region 7.5–10.0 GeV/c		
0.025–0.050	218 ±67	11	0.1487
0.050–0.100	119 ±37	11	0.1358
0.100–0.150	117 ±38	10	0.1255
0.150–0.250	32 ±14	5	0.1159
0.250–0.350	25 ±15	3	0.0867
0.350–0.500	7.7 ± 7.7	1	0.0638
		41	

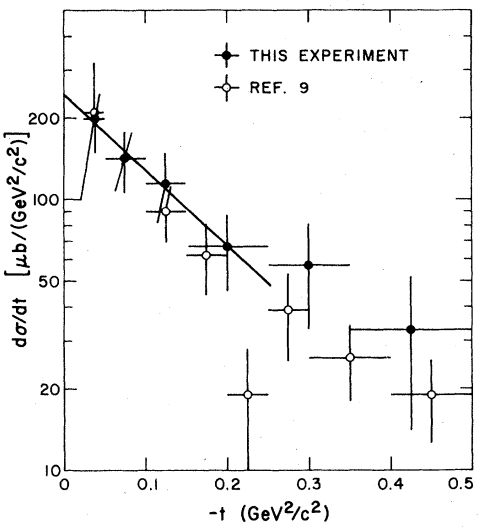

FIG. 4. Differential cross section for the reaction $K_L p \to K_S p$ from 5- to 7.5-GeV/c incident momentum. The line is a fit to the form $d\sigma/dt = (d\sigma/dt)_0\, e^{bt}$ to the four solid circles for the $|t|$ region 0.025–0.25 (GeV/c)^2, giving a slope of 6.4 ± 2.4 (GeV/c)$^{-2}$ and an intercept of 242 ± 65 μb/(GeV/c)^2.

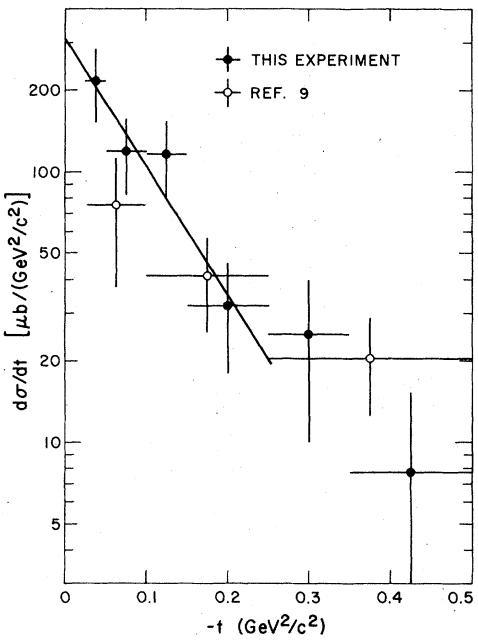

FIG. 5. Differential cross section for the reaction $K_L p \to K_S p$ from 7.5- to 10-GeV/c incident momentum. The line is a fit to the form $d\sigma/dt = (d\sigma/dt)_0\, e^{bt}$ to the four solid circles for the $|t|$ region 0.025–0.25 (GeV/c)^2, giving a slope of 10.8 ± 3.1 (GeV/c)$^{-2}$ and an intercept of 310 ± 103 μb/(GeV/c)^2.

sidered. Incident K_L momenta between 5 and 10 GeV/c were accepted. The values of the momentum-transfer squared (actually $|t|$) accepted were above 0.025 (GeV/c)^2, which corresponds to a proton length of about 1.5 cm. Below this length the scanning efficiency varied with the quality of the film and was poor. Above this length the scanning efficiency was relatively constant at 94%. No events were detected with a $|t|$ value above 0.5 (GeV/c)^2. Additional cuts required that the recoil proton occur in the ±16-cm fiducial region of the chamber (visible region), and the distance of the K_S decay from the vertex was greater than 0.3 cm and less than 25 cm. Below 0.3 cm, the $K_S p$ topology was difficult to separate from three-prong topologies such as $K_L p \to K^+ \pi^- p$. Above 25 cm, the scanning efficiency again was poor. After all these requirements were applied, the data were quite clean. The background from $K_L p \to K_L p$ and $\bar{K}^0 p \to \Lambda^0 \pi^+$ was shown to be less than 1% each.

The number of events observed and the detection efficiency are presented in Table II. In addition, these results are shown in Figs. 4 and 5 and compared with a previous measurement.[9] The solid line is a fit to the experimental data in the region $|t|$ from 0.0 to 0.25. Table III summarizes the t dependence and intercept $(d\sigma/dt)_0$ for the data parametrized as $d\sigma/dt = (d\sigma/dt)_0 e^{bt}$. The same quan-

TABLE III. Determination of the phase of the forward amplitude for $K_L p \to K_S p$.

P (GeV/c)	Slope [(GeV/c)$^{-2}$]	$\left(\frac{d\sigma}{dt}\right)_0$ [μb/(GeV/c)^2]	$\left(\frac{d\sigma}{dt}\right)_{opt}$ [μb/(GeV/c)^2] [a]	$\frac{\mathrm{Re}A}{\mathrm{Im}A}$	ϕ (degrees)	$\alpha(0)$
5 – 7.5	6.4 ± 2.4	242 ± 65	177 ± 19	0.61 ± 0.32	-121 ± 14	0.35 ± 0.24
7.5 – 10	10.8 ± 3.1	310 ± 103	112 ± 14	1.33 ± 0.36	-143 ± 7.6	0.59 ± 0.13
Weighted average this experiment:				0.93 ± 0.24	-138 ± 7.0	0.54 ± 0.11
Weighted average Ref. 9:				0.92 ± 0.13	-133.9 ± 4.0	0.49 ± 0.05
Weighted average Ref. 10:					-132.3 ± 5.7	

[a] Value from Ref. 9.

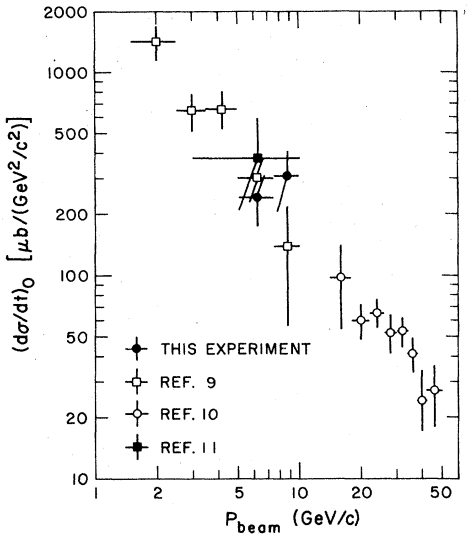

FIG. 6. The value of the differential cross section at $t=0$ as a function of the beam momentum.

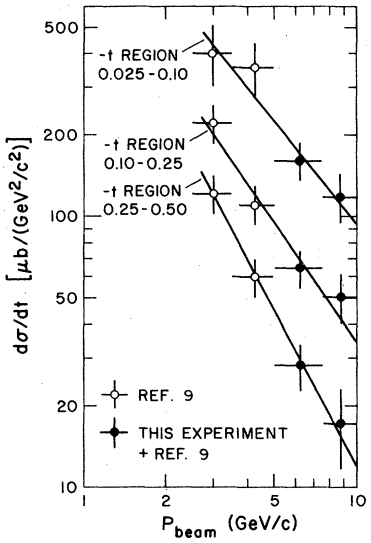

FIG. 8. Energy dependence of the differential cross section for different t intervals, fitted to $d\sigma/dt = Ap^{2\alpha-2}$.

tity has also been measured with coherent regeneration experiments[10] yielding the values in Fig. 6.

From the optical theroem and isospin invariance one can show that

$$\mathrm{Im}A(K_L p \to K_S p)_0 = k/8\pi(\sigma_{K^+n} - \sigma_{K^-n}) ,$$

where k is the incident momentum. With this relation and a determination of $(d\sigma/dt)_0$ we obtain the relation

$$\left(\frac{\mathrm{Re}A}{\mathrm{Im}A}\right)_{t=0} = \left[\frac{(d\sigma/dt)_0}{(\mathrm{Im}A)_0^2} - 1\right]^{1/2} = \left[\frac{(d\sigma/dt)_0}{(d\sigma/dt)_{\text{optical}}} - 1\right]^{1/2} .$$

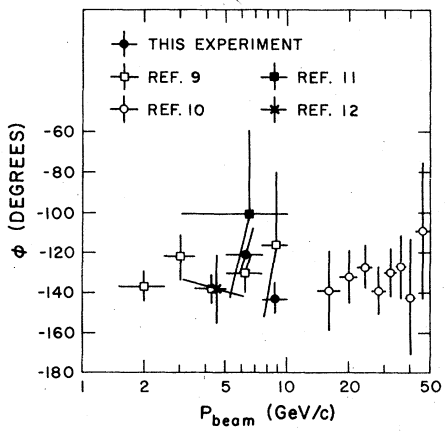

FIG. 7. The phase of the $K_L p \to K_S p$ scattering amplitude at $t=0$ as a function of the beam momentum.

The values of this ratio are shown in Table III. Since $\sigma_{K^-n} > \sigma_{K^+n}$ at our energies, it follows that the phase of the amplitude $\phi = \tan^{-1}(\mathrm{Im}A/\mathrm{Re}A)_0$ must be greater than π. The Regge parameter

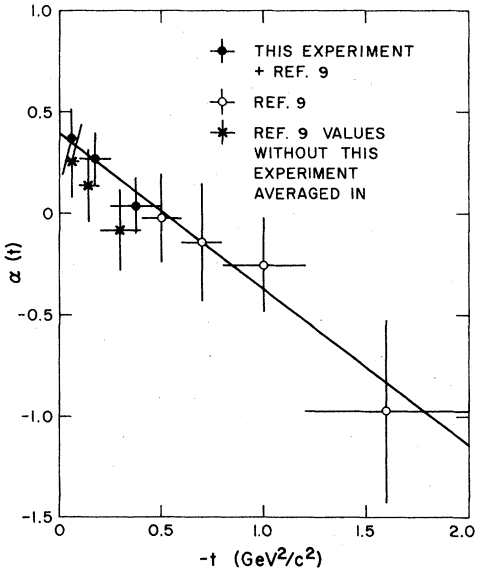

FIG. 9. The ω trajectory, resulting from fit to differential cross sections using $d\sigma/dt \propto p_{\text{lab}}^{2\alpha(t)-2}$, plotted versus t. A straight-line fit to the solid and open circles yields an intercept of 0.39 ± 0.10 and a slope of 0.76 ± 0.21 (GeV^2/c^2)$^{-1}$.

$\alpha(0)$ is related to ϕ by the relation $\phi = -\frac{1}{2}\pi[\alpha(0) + 1]$. Experimentally, we and others have determined that $\alpha(0)$ lies between 0 and 1. Hence we choose ϕ to be in the third quadrant. The value of ϕ is presented in Table III and is plotted with other determinations[9-11] in Fig. 7. The resultant value of $\alpha(0)$ is 0.54 ± 0.11 and is also summarized in Table III.

We finally combined our results with those of Ref. 9 in order to determine the Regge-trajectory parameter $\alpha(t)$ via the Regge relationship $d\sigma/dt = Ap^{2\alpha(t)-2}$. The 10% stated systematic uncertainty in the cross sections of Ref. 9 is added in quadrature with their statistical errors. Above 5 GeV, where both experiments had data, a weighted average of the cross sections was made. The energy- and momentum-transfer dependence of the differential cross section is presented in Fig. 8. The resultant Regge trajectory is shown in Fig. 9. The linearity of α versus t is very good. A straight-line fit gives an intercept of 0.39 ± 0.10 and a slope of (0.76 ± 0.21) $(\mathrm{GeV}/c)^{-2}$. The value of $\alpha(0)$ determined this way is in agreement with the value determined using the phase.

ACKNOWLEDGMENTS

We would like to thank J. Ballam, R.D. Watt, the RCBC staff, and SLAC personnel for their support in this experiment. Also we thank the scanning and measuring staffs at SLAC and the University of Colorado for their many hours of hard work. This work was carried out with the support of the U.S. Department of Energy.

---

*Present address: Fermi National Accelerator Laboratory Batavia, Illinois 60510.
†Present address: Hewlett-Packard, Palo Alto, California.
‡Present address: University of Wisconsin, Physics Department, Madison, Wisconsin 53706.
§Present address: California Institute of Technology, Pasadena, California 91125.
||Present address: Global Union Bank, New York, New York.
¶Present address: Systems Control, Inc., Palo Alto, California.
**Present address: Stanford Linear Accelerator Center, Stanford, California 94305.

[1]A. V. Barnes, D. J. Mellema, A. V. Tollestrup, R. L. Walker, O. I. Dahl, R. A. Johnson, R. W. Kenney, and M. Pripstein, Phys. Rev. Lett. 37, 76 (1976); O. I. Dahl, R. A. Johnson, R. W. Kenney, M. Pripstein, A. V. Barnes, D. J. Mellema, A. V. Tollestrup, and R. L. Walker, *ibid.* 37, 80 (1976); G. Höhler, J. Baacke, H. Schlaile, and P. Sonderegger, Phys. Lett. 20, 79 (1966).
[2]F. J. Gilman, Phys. Rev. 171, 1453 (1968).
[3]C. A. Levinson, N. S. Wall, and H. J. Lipkin, Phys. Rev. Lett. 17, 1122 (1966).
[4]R. Coombes, D. Fryberger, D. Hitlin, R. Piccioni, D. Porat, and D. Dorfan, Nucl. Instrum. Methods 98, 317 (1972). See also R. Piccioni, G. Donaldson, D. Fryberger, D. Hitlin, J. Liu, B. Meyer, A. Rothenberg, M. Schwartz, D. Uggla, S. Wojcicki, D. Dorfan, and R. Messner, Phys. Rev. D 9, 2939 (1974).
[5]J. Ballam and R. D. Watt, Annu. Rev. Nucl. Sci. 27, 75 (1977).
[6]More detailed information is given in M. J. Mugge, Ph.D. thesis, University of Colorado, Boulder, Colorado, 1977 (unpublished).
[7]R. Coombes, D. Hitlin, D. Porat, K. Anderson, D. McQuate, R. Morse, M. Mugge, G. Schultz, P. Cowell, and J. Dorfan, IEEE Trans. Nucl. Sci. 22, 292 (1975).
[8]The Monte Carlo simulation was adapted from a previous experiment using the K^0 spectrometer [R. Messner, R. Morse, U. Nauenberg, D. Hitlin, J. Liu, R. Piccioni, M. Schwartz, S. Wojcicki, and D. Dorfan, Phys. Rev. Lett. 30, 876 (1973)].
[9]G. W. Brandenburg, W. B. Johnson, D. W. G. S. Leith, J. S. Loos, G. J. Luste, J. A. J. Matthews, K. Moriyasu, W. M. Smart, F. C. Winkelmann, and R. J. Yamartino, Phys. Rev. D 9, 1939 (1974).
[10]V. K. Birulev *et al.*, Nucl. Phys. B115, 249 (1976).
[11]C. D. Buchanan, D. J. Drickey, F. D. Rudnick, P. F. Shepard, D. H. Stork, H. K. Ticho, C.-Y. Chien, B. Cox, L. Ettlinger, L. Resvanis, R. A. Zdanis, E. Dally, E. Seppi, and P. Innocenti, Phys. Lett. 37B, 213 (1971).
[12]P. Darriulat, C. Grosso, M. Holder, J. Pilcher, E. Radermacher, C. Rubbia, M. Scire, A. Staude, and K. Tittel, Phys. Lett. 33B, 433 (1970).